# Modelling the strength and stiffness behavior of coarse-grained soils using 3D printed soil analogs

<sup>1</sup>Alejandro Martinez, <sup>2</sup>Sheikh Sharif Ahmed,

<sup>2</sup>Civil and Environmental Engineering, University of California Davis, United States, amart@ucdavis.edu

<sup>1</sup>Group Delta Consultants, Inc., United States, sheikha@groupdelta.com

### ABSTRACT

Inherent particle properties such as size, shape, gradation, surface roughness and mineralogy govern the mechanical behavior of coarse-grained soils. Obtaining a detailed understanding of soil behavior requires parametrization of the individual effects of these properties; however, isolating these effects is a challenge in experimental studies. The advances in 3D printing technology provide the ability to generate artificial sand- and gravel-sized particles with independent control over their size, shape, and gradation. This paper summarizes the strength and stiffness behavior of specimens composed of 3D printed (3DP) particles. Specifically, results of triaxial compression and bender element tests on 3DP sands are provided and compared to corresponding results on the natural sands. The 3DP sands show characteristic behaviors of natural sands, such as dependence on effective stress and stress-dilatancy. However, the 3DP soils are more compressible due to the smaller stiffness of the constituent polymeric material. The results show a decrease in critical state friction angle ( $\varphi'_{cs}$ ) and an increase in shear wave velocity ( $V_s$ ) as the particle roundness and sphericity are increased, in agreement with published trends for natural soils. The agreement in trends highlights the potential for investigations using 3DP soils to extend the understanding of soil behavior.

**Keywords:** 3D printing, soil analog, particle shape, triaxial compression, shear wave velocity.

# 1 INTRODUCTION

Performing parametric studies on the effect of inherent properties, such as particle size and shape, gradation, and mineralogy, on the response of soil specimens is required to better understand the behavior of soils and to develop and validate constitutive models. However, isolating the effects of these properties is an experimental challenge. Recent advancements in 3D printing technology allow generating particles that accurately reproduce the morphology of sand- and gravel-sized particles. These soil analogs have been used to investigate the permeability of uniformly graded soils, effect of particle shape on strength, stiffness, and clogging, frictional interactions at faults, and to validate DEM simulations (e.g. Hanaor et al. 2016; Matsumura et al. 2017; Adamidis et al. 2020; Hafez et al. 2021; Gupta et al. 2019). The response of 3DP soils has been shown to exhibit some of the fundamental behaviors of natural coarse-grained soils, including effective stressdependency of strength and stiffness and stress-dilatancy (e.g. Hanaor et al. 2016; Matsumura et al. 2017; Ahmed and Martinez 2020, 2021).

### 2 MATERIALS AND METHODS

# 2.1 3D printed sands

The 3DP particles were printed using an Objet Eden 260V printer from Statasys with VeroWhitePlus rigid acrylate-based polymer resin. This printer uses an additional water-soluble resin to create removable support structures. The VeroWhitePlus polymer has a Young's modulus of 2.4 GPa, Poisson's ratio of 0.3, and specific gravity of 1.18. The particles were printed using a layer thickness of 30  $\mu$ m. Ahmed and Martinez (2020, 2021) provide a detailed description of the procedures employed for printing and processing as well as a discussion of the implications of the differences in material properties between the polymer and natural minerals on the behavior of soil specimens.

This investigation considered seven 3DP mixes. The particle morphology of Mixes 3, 6, 7, and 8 were generated using the method proposed by Wei et al. (2018) that uses spherical harmonics to create 3D shapes based on target shape parameters (Ahmed and Martinez 2022). Mix 1 consisted of equal-sized spheres. Mixes 2 and 4 were printed from X-ray CT scans of natural

rounded and angular particles. Fig. 1a and 1b show a comparison of X-ray CT scans of the natural and 3DP particles, showing the greater layering of the latter produced during the printing process. Ahmed and Martinez (2021) provide a detailed discussion of the effects of this surface texture on the contact forcedeformation response and friction coefficient. The 3D printing process was found to successfully reproduce the shape parameters of the natural sand particles, as presented in Fig. 1c where the difference in shape parameter values between natural and 3DP particles is negligible. Table 1 provides the particle shape parameters for the seven 3DP mixes, where the circle ratio sphericity ( $S_C$ ) is the ratio of the diameter of the largest inscribed circle to the diameter of the minimum circumscribing circle, and the regularity  $(R_G)$  is the average R and  $S_C$ . All the 3DP mixes were poorlygraded, Mixes 1, 2, and 4 had mean particle sizes  $(D_{50})$ of 3.2 mm, and Mixes 3, 5, 6, and 7 had  $D_{50}$  of 2.5 mm.

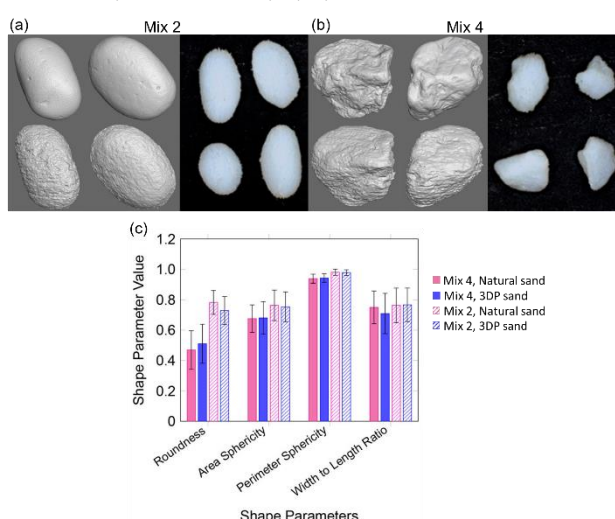


Fig. 1. (a) Mix 2: X-ray CT of natural (top) and 3DP (bottom) particles and photograph of 3DP particles. (b) Mix 4: X-ray CT of natural (top) and 3DP (bottom) particles and photograph of 3DP particles. (c) Comparison of particle shape parameters of natural and 3DP sands (brackets indicate standard deviation magnitudes).

Table 1. Average particle shape parameters of 3DP mixes (numbers in parenthesis indicate standard deviations).

-	Soil specimen	Wadell roundness, R	Circle ratio sphericity $S_{\rm C}$	Regularity, $R_{\rm G}$
_	Mix 1	0.90 (0.09)	0.94 (0.01)	0.92 (0.05)
	Mix 2	0.73 (0.09)	0.75 (0.10)	0.74 (0.08)
	Mix 3	0.61 (0.12)	0.75 (0.04)	0.68 (0.07)
	Mix 4	0.52 (0.13)	0.66 (0.10)	0.59 (0.08)
	Mix 6	0.55 (0.13)	0.65 (0.05)	0.60(0.07)
	Mix 7	0.48 (0.12)	0.53 (0.04)	0.50 (0.06)
	Mix 8	0.54 (0.11)	0.84(0.04)	0.69(0.07)

### 2.1 Triaxial and bender element testing

A series of 30 isotropically-consolidated drained triaxial (ICD TX) compression tests were performed on saturated specimens of Mixes 2, 3, 4, 6, 7, and 8 using an automated triaxial testing equipment. The specimens

of Mixes 2 and 4 had dimensions of 70 mm in diameter and 150 mm in height, while the specimens of Mixes 3, 6, 7, and 8 had a diameter of 35 mm and a height of 71 mm. All specimens were prepared to loose conditions at relative densities  $(D_R)$  between 10 and 20% to avoid shear banding. The specimens were back-pressure saturated to a B-value greater than 0.95. The specimens were consolidated to target confining pressures  $(\sigma'_3)$  between 20 and 90 kPa before they were sheared to axial strains of 30% or greater. It is noted that consolidation of all the specimens resulted in reduction of the void ratio (e) and  $D_R$  owing to the compressibility of the polymer. Ahmed and Martinez (2021) provide a more detailed description of the triaxial testing procedure and methods.

Bender element (BE) tests were performed on dry specimens of all seven mixes. The setup consists of top and bottom acrylic caps with BEs embedded on them, which are used to send and receive shear waves along the specimen's height. The specimens were contained in latex membranes and had a diameter of 70 mm and heights between 65 and 75 mm. Mean effective stresses (p') between 10 and 80 kPa were applied using vacuum.  $V_s$  measurements were determined from the received signals using the arrival time determined using the initial rise criterion. Ahmed and Martinez (2020) provide a detailed description of the methods used for BE testing.

# 3 TRIAXIAL COMPRESSION TESTS ON 3DP SANDS

Triaxial compression tests were performed at  $\sigma'_3$  of 20, 30, 50, 70, and 90 kPa. The deviatoric stress (q) increased as  $\sigma'_3$  was increased, and the stress paths followed 3:1 slopes in q-p' space. Fig. 2a and 2c show the results for Mix 6; the other mixes showed the same trends but are not included here for brevity. The reader is referred to Ahmed and Martinez (2021) and Ahmed (2021) for the complete dataset and for a comparison of the behavior of Mixes 2 and 4 with that of natural sands with the same morphology. All specimens exhibited an contraction followed by mild characteristic of loose materials (Fig. 2b and 2d). The specimens confined to greater  $\sigma'_3$  had smaller initial void ratios due to their greater compression, leading to smaller amounts of contraction.

The q and p' at large strains (> 30%) were used to estimate critical state points and define the critical state lines (CSLs) for all the mixes (Fig. 3). The CSLs appear to be curved, which may be due to the pressure-dependency of the inter-particle friction coefficient ( $\mu$ ) of the printed polymer. Indeed, Ahmed and Martinez (2021) reported a decrease in  $\mu$  with increasing effective stress. In the analysis presented here, the CSLs are approximated by fitting lines to two different  $\sigma'_3$  ranges. The CSLs fitted at  $\sigma'_3$  smaller than 50 kPa have a greater slope than the lines fitted at greater  $\sigma'_3$  for all soil mixes.

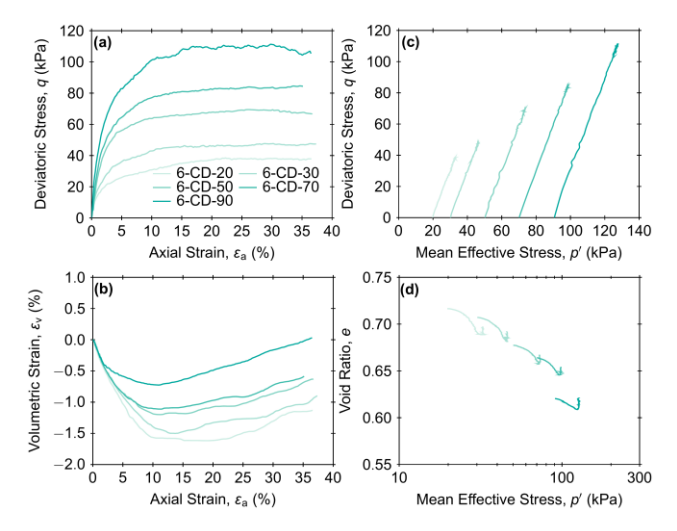


Fig. 2. Triaxial compression tests on Mix 6: (a) deviatoric stress - axial strain, (b) volumetric strain - axial strain, and stress paths in (c) stress and (d) compression planes.

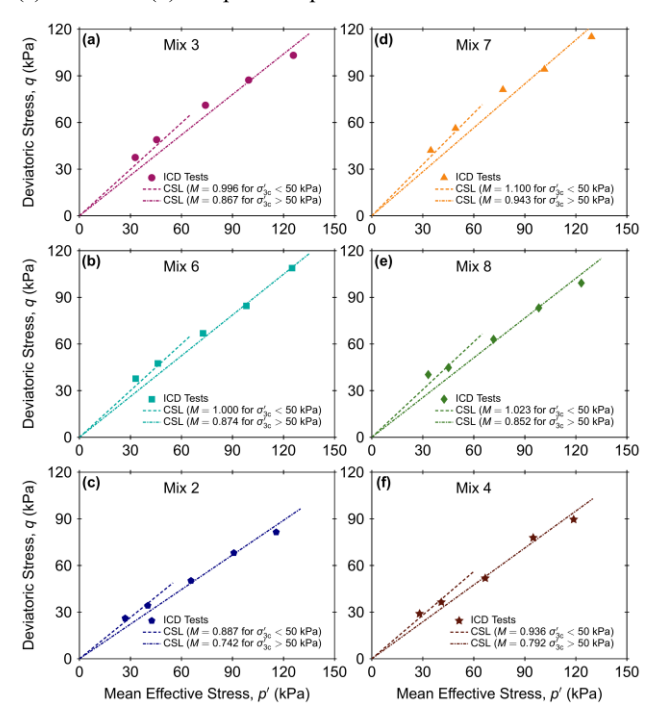


Fig. 3. Critical state lines in q-p' space for Mixes (a) 3, (b) 6, (c) 2, (d) 7, (e) 8, and (f) 4.

The slope of the CSLs (M) was used to compute critical state friction angles ( $\phi'_{cs}$ ) for the six soil mixes. The results indicate a decrease in  $\phi'_{cs}$  with increasing roundness, sphericity, and regularity. For example, for  $\sigma'_3$  smaller than 50 kPa, Mix 7 with the smallest R,  $S_C$ , and  $R_G$  exhibits the greatest  $\phi'_{cs}$  of 25.6° while Mix 2 with the greatest R,  $S_C$ , and  $R_G$  exhibits the smallest  $\phi'_{cs}$  of 22.7°. The measured  $\phi'_{cs}$  are plotted as a function of R,  $S_C$ , and  $R_G$  in Fig. 4, which also provides values from natural sands reported in the literature. The reader is referred to Ahmed (2021) for the complete list and references of these literature values. The relationship between  $\phi'_{cs}$  and R,  $S_C$ , and  $R_G$  can be fitted with a line

for both 3DP and natural sands. The lines for 3DP and natural sands have comparable slopes, indicating that the effect of particle shape in the change of  $\phi'_{cs}$  can be reasonably captured by the 3DP soils. However, the intercepts of the lines are smaller for the 3DP soils, indicating that the absolute  $\phi'_{cs}$  values may need to be corrected to account for differences in factors such as  $\mu$  and compressibility.

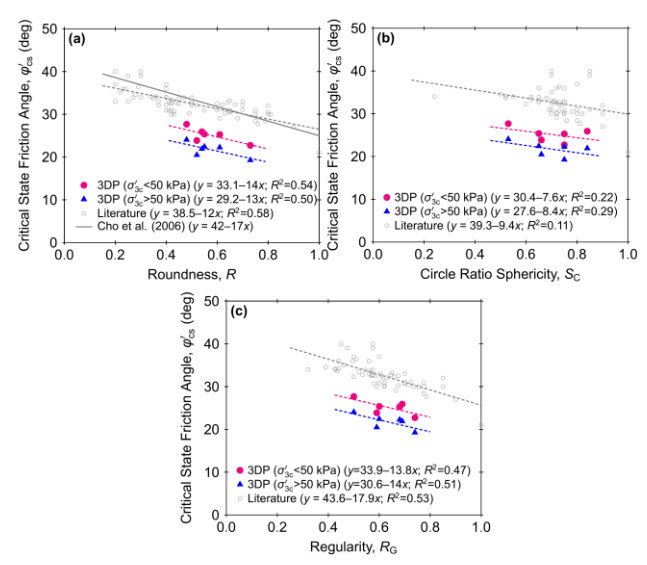


Fig. 4. Relationship between  $\varphi'_{cs}$  with (a) R, (b)  $S_C$ , and (c)  $R_G$ , along with comparison to values from the literature.

### 4 BENDER ELEMENT TESTS ON 3DP SANDS

Shear wave velocity measurements were obtained with the BEs on specimens with e of 0.55 and 0.65 (Fig. 5). The  $V_s$  magnitude increased with increasing p' for both the specimens. The results are fitted with power-law relationships with the form  $V_s = \alpha p'^{\beta}$ , which provide high quality fits as evidenced by the large  $R^2$  values.  $V_s$  increase as the R,  $S_C$ , and  $R_G$  are increased for any given e and p'. For example, the  $V_s$  values for Mix 1 with the greatest R,  $S_C$ , and  $R_G$  are the highest, while the  $V_s$  measurements for Mix 7 with the smallest R,  $S_C$ , and  $R_G$  have the smallest magnitudes. Consistent trends are obtained if the  $V_s$  of specimens with similar relative densities are compared.

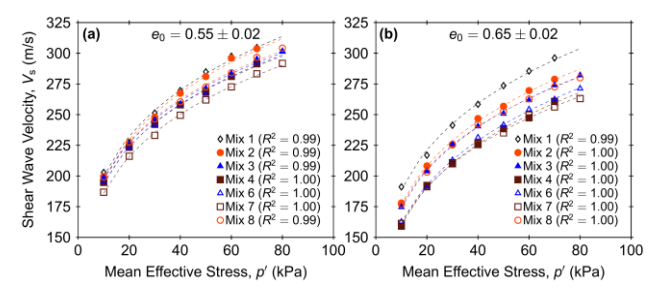


Fig. 5.  $V_s$  measurements as a function of p' for the 3DP mixes.

To further examine the effect of particle shape, Fig. 6 presents  $V_s$  values as a function of the shape parameters

for specimens subjected to p' of 50 kPa and with e of 0.55 and 0.65. As shown, the  $V_s$  increases in a non-linear fashion as R,  $S_C$ , and  $R_G$  are increased. This trend is in agreement with those from investigations on natural sands by Cho et al. (2006), Patel et al. (2009), and Lee et al. (2017). The  $R^2$  values are greatest for the relationship with  $R_G$  (Fig. 6c), and they are smallest for the relationship with  $S_C$  (Fig. 6b), suggesting that  $R_G$  is more strongly correlated to  $V_s$  than  $S_C$ .

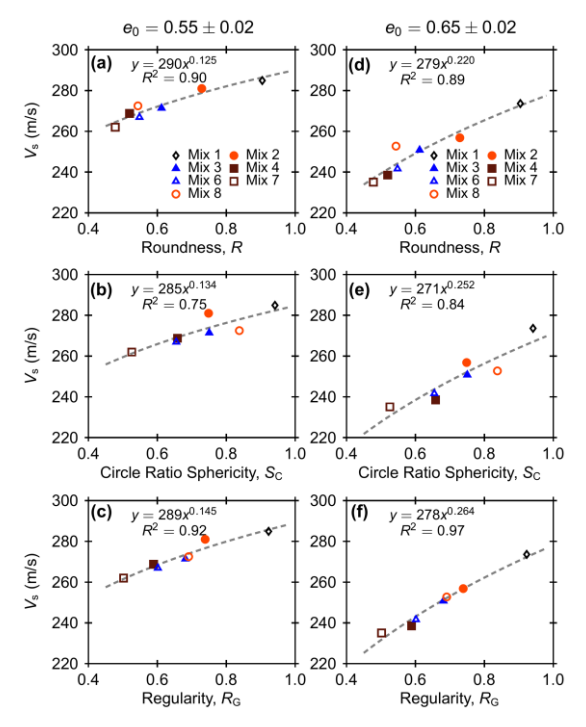


Fig. 6.  $V_s$  as a function of (a) R, (b)  $S_C$ , and (c)  $R_G$  for specimens with e = 0.55, and as a function of (d) R, (e)  $S_C$ , and (f)  $R_G$  for specimens with e = 0.65 (p' = 50 kPa).

# 5 CONCLUSIONS

3D printed soils are promising analog materials that allow to isolate the effects of individual particle properties, such as size, shape, and constituent material, on the response specimens. A range of 3D printing technologies have been used to date to print particles in the size range of medium sands to gravels with accurate reproduction of particle shapes. This paper presents the results of triaxial compression and bender element tests on seven 3DP soil mixes with varying particle shapes.

The results of ICD TX tests indicate that the 3DP soils exhibit behaviors characteristic of natural coarse-grained soils, including effective stress-dependency on shear strength and stress-dilatancy. Tests at different cell pressures were performed to define the CSLs in q-p' space for six of the soil mixes, which allow computing  $\phi'_{cs}$  values. The  $\phi'_{cs}$  of the 3DP soils are shown to decrease with increasing particle roundness and sphericity at a similar rate as those of natural sands.

Aspects of the behavior of 3DP sands that differ from those of natural sands include the greater compression during consolidation and the smaller  $\phi'_{cs}$  magnitudes, which are due to the greater compressibility and smaller interparticle friction coefficient of the 3DP polymer.

The results of the BE tests indicate that the 3DP soils exhibit a non-linear increase in  $V_s$  with mean effective stress that can be well-fitted with a power law equation. The  $V_s$  at any given void ratio and effective stress was shown to increase with increasing roundness and sphericity, in agreement with previously published trends for natural soils. Particle regularity had a stronger correlation with  $V_s$  than roundness and sphericity.

### **ACKNOWLEDGEMENTS**

This material is based upon work supported by the National Science Foundation (NSF) under award No. 1735732. Any opinions, findings, and conclusions expressed in this material are those of the author(s) and do not necessarily reflect those of the NSF.

### REFERENCES

Adamidis O., Alber S. and Anastasopoulos I. (2020). Assessment of three-dimensional printing of granular media for geotechnical applications. *Geotechnical Testing J.* 43(3).

Ahmed, S. 2021. Study of particle shape, size, and gradation effects on the mechanical behavior of coarse-grained soils. PhD dissertation, University of California Davis.

Ahmed S.S. and Martinez A. 2020. Modeling the mechanical behavior of coarse-grained soil using additive manufactured particle analogs. *Acta Geotechnica* 15(10), 2826-2847.

Ahmed S.S. and Martinez A. 2021. Triaxial compression behavior of 3D printed and natural sands. *Granular Matter* 23, 1-21.

Ahmed S.S. and Martinez A. 2022. Effects of Particle Shape on the Shear Wave Velocity and Shear Modulus of 3D Printed Sand Analogs. *Open Geomechanics* 3, 1-18.

Cho G.-C., Dodds J. and Santamarina J. C. 2006. Particle shape effects on packing density, stiffness, and strength: Natural and crushed sands. *Journal of Geotechnical and Geoenvironmental Engineering* 132(5), 591–602.

Gupta R., Salager S., Wang K. and Sun W.C. 2019. Open-source support toward validating and falsifying discrete mechanics models using synthetic granular materials. *Acta Geotechnica* 14(4), 923–937.

Hanaor D., Gan Y., Revay M., Airey D. and Einav I. 2016. 3d printable geomaterials. *Geotechnique* 66(4), 323–332.

Lee C., Suh H. S., Yoon B., and Yun T. S. 2017. Particle shape effect on thermal conductivity and shear wave velocity in sands. *Acta Geotechnica* 12(3), 615–625.

Matsumura S., Kobayashi T., Mizutani T. and Bathurst R. J. 2017. Manufacture of bonded granular soil using X-ray CT scanning and 3D printing. *Geotechnical Testing J.* 40(6), 1000–1010.

Patel A., Bartake P. and Singh, D. 2009. An empirical relationship for determining shear wave velocity in granular materials accounting for grain morphology. *Geotechnical Testing Journal* 32(1), 1–10.

Wei D., Wang J. and Zhao B. 2018. A simple method for particle shape generation with spherical harmonics. *Powder Technology* 330, 284–291.